Published in final edited form as:
Sci Transl Med. 2011 April 20; 3(79): . doi:10.1126/scitranslmed.3001963.

THE FATE AND TOXICITY OF RAMAN ACTIVE SILICA-GOLD NANOPARTICLES IN MICE

AVNESH S THAKOR[1,3], **RICHARD LUONG**[2], **RAMASAMY PAULMURUGAN**[1], **FRANK I LIN**[1], **PAUL KEMPEN**[4], **CRISTINA ZAVALETA**[1], **PAULINE CHU**[2], **TARIK F MASSOUD**[1,3], **ROBERT SINCLAIR**[4], and **SANJIV S GAMBHIR**[1,4,5]

[1]Molecular Imaging Program at Stanford, Department of Radiology, Stanford University, California, 94305-5427, USA

[2]Department of Comparative Medicine, Stanford University, California, 94305-5410, USA

[3]Department of Radiology, University of Cambridge, Cambridge, CB2 2QQ, UK

[4]Department of Materials Sciences & Engineering, Stanford University, California, 94305-4034, USA

[5]Department of Bioengineering and Bio-X Program, Stanford University, California, 94305-5427, USA

Abstract

Raman spectroscopy is an optical imaging modality which analyses the Raman effect in which energy is exchanged between light and matter. Although Raman spectroscopy has been widely used for chemical and molecular analysis, its use in clinical applications has been hindered by the inherently weak nature of the Raman effect. Raman-silica-gold-nanoparticles (R-Si-Au-NPs) overcome this limitation by producing high Raman signals via Surface Enhanced Raman Scattering. Targeted polyethylene glycol (PEG)-ylated R-Si-Au-NPs (e.g. PEG-R-Si-Au-NPs labeled with an affibody which binds specifically to the epidermal growth factor receptor) are currently being designed to detect colorectal cancer after administration into the bowel lumen. With this approach, PEG-R-Si-Au-NPs are not expected to enter the systemic circulation and would be removed from the body via defecation. We examined the acute toxicity and biodistribution of core PEG-R-Si-Au-NPs after different routes of administration in mice. After *intravenous* administration, PEG-R-Si-Au-NPs were removed from the circulation by marcophages in the liver and spleen (i.e. the reticuloendothelial system). At 24 hours, PEG-R-Si-Au-NPs elicited a mild inflammatory response and an increase in oxidative stress in the liver, which subsided by 2 weeks. No evidence of significant toxicity was observed by measuring clinical, histological, biochemical or cardiovascular parameters for 2 weeks. Notably, after administration *per rectum,* we observed no significant bowel or systemic toxicity and no PEG-R-Si-Au-NPs were detected systemically. Although additional studies are required to investigate the long-term effects of PEG-R-Si-Au-NPs, these initial results support the idea that they can be safely used in living subjects, especially when administered *rectally*.

Corresponding Author: Sanjiv S Gambhir, MD PhD, Director, Molecular Imaging Program at Stanford (MIPS), The James H Clark Center, 318 Campus Drive, Stanford, CA 94305-5427, sgambhir@stanford.edu Fax: 650-724-4948.

Author Contributions: A.S.T. designed and performed all experiments, analyzed all the data and wrote the paper; R.L. histological experiments and data analysis; R.P. gene expression experiments and data analysis; F.I.L. ICP-MS experiments and data analysis; P.K. STEM experiments and data analysis; C.Z. designed and performed experiments; P.C. Immunohistochemistry and TUNEL assay experiments; T.F.M. designed experiments and help write the paper; R.S. STEM experiments; S.S.G. designed all experiments, analyzed all the data and wrote the paper

Competing interests: None

INTRODUCTION

Non-invasive molecular imaging allows the study of cellular and metabolic processes in living subjects in real time. This new emerging field has the potential to play a central role in many areas of biomedical research and clinical patient management including patient screening via the detection of disease specific molecular markers, selecting disease and patient specific treatment and measuring the molecular responses following treatment (1–3). Current clinical molecular imaging approaches use positron emission tomography (PET) or single photon emission computed tomography (SPECT). However, there are several new multi-modality molecular imaging technologies being explored pre-clinically. These include ultrasound (US) with molecularly targeted microbubble contrast agents, magnetic resonance spectroscopy (MRS), photoacoustic imaging and optical imaging using either fluorescent molecular probes or Raman spectroscopy (4). However, no single molecular imaging modality meets all the criteria required for translation into everyday clinical practice: high sensitivity and specificity, high spatial and temporal resolution, multiplexing, safety, acceptability and low cost.

Pre-clinical medical imaging of small animals using optical spectroscopy has traditionally relied on fluorescence, however, its potential for *in vivo* applications has been limited by (i) the small number of fluorescent imaging agents available in the near infra-red spectrum, which thus limits the use of low energy lasers to interrogate specimens (ii) high background autofluorescence from superficial tissues, which restricts the sensitivity and depth of this imaging modality (iii) the large spectral overlap between fluorescent imaging agents, which prevents the detection of multiple targets simultaneously (multiplexing) and (iv) the rapid photobleaching of fluorescent molecules, which limits study duration (5, 6). Optical spectroscopy using the Raman effect has shown great promise in overcoming many of these limitations.

The Raman effect describes how energy is exchanged between light and matter. When light impinges on a substance, it can be either absorbed or scattered. Since the energy of light is proportional to its frequency, most of the scattered light will have the same frequency as that of the incident light. However, a small fraction of the incident light can transfer some of its energy into setting some molecules from their ground state into an excited vibrational state. This is accompanied by the simultaneous absorption of the incident photon and the emission of a Raman scattered photon. The energy exchange, and hence frequency shift, between the incident photon and Raman scattered photon is known as the Raman effect (7). In recent years Raman spectroscopy has proven to be an invaluable bioanalytical tool, having the ability to differentiate the spectral fingerprint of many molecules, thereby allowing the chemical composition of tissues to be determined with high sensitivity and minimal sample preparation (8–10). Furthermore as light can be rapidly delivered and collected by optical fibers, Raman spectroscopy has the potential to be performed *in vivo*, in real time, when incorporated into catheters and endoscopes (7). However, magnitude of the Raman Effect is inherently weak (ca. 1 photon is inelastically scattered for every 10^7 elastically scattered photons) which limits the sensitivity and hence the clinical applications of Raman spectroscopy.

In recent years, advances in nanobiotechnology have enabled the synthesis of a Raman-silica-gold-nanoparticle (R-Si-Au-NP) which can overcome this problem by taking advantage of the phenomenon known as surface enhanced Raman scattering (SERS). SERS is a plasmonic effect where molecules adsorbed onto a nano-roughened noble metal surface experience a dramatic increase in the incident electromagnetic field, thereby resulting in high Raman intensities (11).

Nanoparticles have been shown to possess very different properties compared to their corresponding bulk material which has implications for their use *in vivo* since their small size will affect their mode of endocytosis, cellular trafficking and processing. In addition, their high surface area to volume ratio, surface reactivity and charge will dramatically alter their chemical and physical properties resulting in them possessing unexpected toxicities and biological interactions. Although several studies have been undertaken to investigate the toxicity associated with nanoparticles, the results are often highly variable, attributed, in part, to the different shapes, sizes and chemical preparations of nanoparticles studied (14–16). In a recent cell culture study, exposure of cultured human cells to PEG-R-Si-Au-NPs at low concentrations (1–100 PEG-R-Si-Au-NPs/cell) caused negligible toxicity. At very high concentrations, minimal cytotoxicty and oxidative stress was observed after prolonged exposure (1000 PEG-R-Si-Au-NPs/cell for 48h) (13). Furthermore, the route of administration can also affect nanoparticle toxicity with several studies demonstrating reduced toxicity following intravenous administration of nanoparticles due to macrophages within the reticuloendothelial system, in particular the liver, efficiently removing low concentrations of nanoparticles from the systemic circulation, thereby minimizing their potential to cause toxicity (17, 18). For these reasons, were are designing PEG-R-Si-Au-NPs to target colon cancer. We hypothesize that these PEG-R-Si-Au-NPs will not cross the bowel-wall when administered *rectally* and that if any do enter the systemic circulation, they would be directed to the liver by the portal venous system where they would be entrapped (17, 18).

In the present study, we have therefore examined in mice whether *rectally* (PR) administered PEG-R-Si-Au-NPs would cause toxicity to the bowel and whether these nanoparticles would cross the bowel-wall. In case any nanoparticles do enter the circulation by crossing the bowel wall, we separately examined the systemic biodistribution and acute effects of directly administered PEG-R-Si-Au-NPs into the circulation via the *intravenous* (IV) route.

RESULTS

Nanoparticle concentration and administration volume

The concentration of PEG-R-Si-Au-NPs (9.6×10^{10} nanoparticles in 200 μl of saline) administered to mice in both the *IV* and *PR* experiments is a 1,000-fold higher dose than the minimum concentration that can be currently detected *in vivo* using a Raman microscope (6). Provided no toxic effects are observed in this study, this single/limit dose is large enough to assess the effects of PEG-R-Si-Au-NPs. However, if significant toxic effects are observed, a graded dose-response analysis would be required. Furthermore, 200 μl of either saline (for control animals) or PEG-R-Si-Au-NPs was small enough volume of fluid to have minimal impact on the animal's cardiovascular system.

General health indices

Male (n=60) and female (n=60) mice were followed daily for 2 weeks after either *IV* or *PR* PEG-R-Si-Au-NP administration. During this time, there were no deaths and no changes were observed in the physical appearance (fur, eyes, mucous membranes, secretions, stool, gait, posture, breathing pattern), behavior (gait, posture, stereotypes, vocalizations) or social interactions of all mice. In both male and female mice, no changes in the electrocardiogram (ECG) (Fig. S1), blood pressure or heart rate (Table S1) occurred after either *IV* or *PR* PEG-R-Si-Au-NP administration. The increase in body weight of all mice receiving PEG-R-Si-Au-NPs over 2 weeks was similar compared to those of control mice, with female mice being slightly lighter than their male counterparts at the start of the study (Table S1). In both

male and female mice, all plasma biochemical and hematological indices remained within their respective normal ranges after *IV* and *PR* PEG-R-Si-Au-NP administration (Table S2).

Gold levels

As the nanoparticle core is made from gold, its biodistribution can be determined by measuring the concentration of gold within tissue samples by inductively coupled plasma mass spectrometry (ICP-MS). Gold was detected in the liver and spleen from male and female mice as early as 5 minutes after *IV* PEG-R-Si-Au-NP administration (Fig. 2). Over the next 2 weeks, there was a gradual decline in the concentration of gold within the liver of male and female animals. In contrast, there was a significant increase in the concentration of gold in the spleen at 24 hours in both sexes compared to the 5 min and 2 hour time points, which gradually decreased over 2 weeks (Fig. 2). Gold was detected in the blood of 1-of-3 female and 2-of-3 male animals 5 min after *IV* PEG-R-Si-Au-NP administration but no gold was detected at later time points. Five minutes after *PR* PEG-R-Si-Au-NP administration, we detected gold in the feces of both male and female mice but we found no gold at later time points. A trace concentration of gold was also detected in a blood sample of a single female mouse at 5 min after *PR* PEG-R-Si-Au-NP and in a lung sample of a single male mouse at 5 min after *IV* PEG-R-Si-Au-NP administration. Examination of the bone marrow, colon, small intestine, kidney, brain, gonads and feces demonstrated no detectable gold following either *IV* or *PR* PEG-R-Si-Au-NP administration in all mice at any time.

Tissue histology

After IV PEG-R-Si-Au-NP administration, detailed necropsy by a mouse pathologist did not reveal any gross organ abnormality or evidence of nanoparticles in the spleen, bone marrow, pancreas, colon, small intestine, heart, kidneys, lungs, brain, and gonads in both male and female animals. However, histological analysis of liver samples 5 min after *IV* PEG-R-Si-Au-NP administration demonstrated very fine black extracellular pigment within the peri-sinusoidal space in both male and female mice (Fig. 3 and S2; Table 1). After 2 hours, similar pigment was also seen intracellularly within resident macrophages of the liver. As the amount of pigment within macrophages increased over 24 hours, less was observed in the sinusoids. By 2 weeks, pigment was only observed within the macrophages, with none present within the liver sinusoids (Fig. 3 and S2; Table 1). No animal demonstrated pigment within hepatocytes at any time point. Twenty-four hours after *IV* PEG-R-Si-Au-NP administration, a mild degree of hepatocellular apoptosis and necrosis was noted within the liver which was no longer evident after 1 week. A slight increase in observable mitotic figures in hepatocytes was also seen in the livers of male and female mice at 24 hours and 1 week after both *IV* saline and PEG-R-Si-Au-NP administration.

After *PR* PEG-R-Si-Au-NP administration, there was no gross organ abnormality or evidence of nanoparticles in the spleen, pancreas, colon, small intestine, heart, kidneys, lungs, brain, and gonads in both male and female animals. Liver tissue from all animals revealed no pigment within the sinusoids, macrophages or hepatocytes at all times examined after PR nanoparticle administration (Fig. 6 and S3; Table 1). Similar to the *IV* experiments, there was mild degree of mitosis within the liver in both male and female mice 1 week after both *PR* saline and PEG-R-Si-Au-NP administration (Fig. 6 and S3; Table 1). A large amount of very fine black pigment was noted within the colonic lumen of all animals at 5 min after PR PEG-R-Si-Au-NP administration, with no pigment subsequently seen within the bowel by 2 hours. Furthermore, no pigment was seen at any time point within the enterocytes of the bowel-wall.

Scanning transmission electron microscopy

Scanning transmission electron microscopy (STEM) was performed to further evaluate the intracellular location of PEG-R-Si-Au-NPs. After *IV* PEG-R-Si-Au-NP administration, STEM analysis of liver samples demonstrated nanoparticles within the macrophages in all animals at each time point of interest. After 5 minutes, majority of PEG-R-Si-Au-NPs were seen within the peri-sinusoidal space with only a small number located within the vesicles of resident macrophages located adjacent to the sinusoids. By 2 hours, the number of nanoparticles internalized by resident macrophages had increased, and by 24 hours, STEM demonstrated large numbers of PEG-R-Si-Au-NPs within the vesicles of macrophages with no PEG-R-Si-Au-NPs detected within the peri-sinusoidal space (Fig. 3 and S2; Movie 1). No PEG-R-Si-Au-NP could be identified with STEM within the liver sinusoids, macrophages or hepatocytes any time point examined after *PR* administration in both male and female mice.

Immunohistochemistry

Immuohistochemical analysis of liver and spleen samples were undertaken to verify the co-localization of PEG-R-Si-Au-NPs with macrophages. However despite two separate attempts by independent laboratories, control and experimental tissues did not react with the monoclonal antibody against the F4/80 macrophage specific antigen.

TUNEL assay

After *IV* PEG-R-Si-Au-NP administration, a representative female animal demonstrated 1 TUNEL-positive cell per 100 counted cells at 2 hours and 24 hours whilst a representative male animal demonstrated 1 TUNEL-positive cell per 100 counted cells at 5 min and 2 TUNEL-positive cells per 100 counted cells at 2 weeks (Table S3). TUNEL-positive cells were identified as those which demonstrated diffuse, brown, intranuclear staining. There were no TUNEL-positive cells in any of the representative liver samples following *PR* PEG-R-Si-Au-NP administration in either sex (Table S3). Furthermore, there were no TUNEL-positive cells identified in the splenic samples after either *IV* or *PR* PEG-R-Si-Au-NP administration in both male and female animals.

Gene expression

After *IV* PEG-R-Si-Au-NP administration, there was an increase in the gene-expression of phase-2 antioxidant enzymes within the liver (Fig. 4). The mRNA levels of catalase and superoxide dismutase both peaked at 1 weak, with the former demonstrating a gradual increase in expression over the preceding time points (Fig. 4). The peak increase in hemoxygenase occurs earlier at 24 hours with gene expression of glutathione peroxidase was maximal at 5 minutes (Fig. 4). The Bax:Bcl-2 ratio, which controls activation of cellular apoptotic effectors, was also significantly increased at 5 min and 2 hours after *IV* PEG-R-Si-Au-NP administration (Fig. 5). In contrast, the expression of TNF-α, IL-6 and caspase all increase significantly later at 24 hours after *IV* PEG-R-Si-Au-NP administration (Fig. 5). By 2 weeks, there was no significant increase in the mRNA of the antioxidant enzymes, pro-inflammatory or pro-apoptotic genes after *IV* PEG-R-Si-Au-NP administration compared to control animals (Fig. 4 and 5).

DISCUSSION

Our results show that *IV* or *PR* PEG-R-Si-Au-NP administration had no effect on the physical appearance, behavior or social interactions in any of the mice studied. Regardless of the route of administration, PEG-R-Si-Au-NPs also had no acute effect on basal cardiovascular function or any of the hematological and biochemical parameters measured.

The results show that the liver and spleen, which are organs of the reticuloendothelial system (RES), can effectively and efficiently remove PEG-R-Si-Au-NPs from the systemic circulation. Histological analysis of liver samples after *IV* PEG-R-Si-Au-NP administration support the ICP-MS data and demonstrate uniform, very fine (<1 micron diameter), black, extracellular pigment within the peri-sinusoidal space (space of Disse) in both male and female mice. This pigment did not histochemically react with the Prussian blue methods, nor the Fontana-Masson method, respectively implying that the pigment was not ferrous-based or melanin-based. Coupled with its uniformly fine diameter and its extracellular location, the pigment was therefore thought to represent the PEG-R-Si-Au-NPs. Scanning transmission electron microscopy of liver samples at early time points demonstrate the presence of PEG-R-Si-Au-NPs within the peri-sinusoidal space with only a small number located within the vesicles of resident macrophages located adjacent to the sinusoids. As time progressed the majority of PEG-R-Si-Au-NPs were found to be internalized by resident macrophages with no PEG-R-Si-Au-NPs detected within the peri-sinusoidal space at the end of the study. Since PEG-R-Si-Au-NPs were mainly located within the sinusoids at the early time points, and not trapped by cellular material, it is possible that there may have been some PEG-R-Si-Au-NP loss during the sample preparation for STEM analysis at these times. Histologically, the spleens of all mice appeared normal, but specific assessment of the spleen for the presence and amount of PEG-R-Si-Au-NPs was inconclusive, primarily due to the presence of the iron-containing hemosiderin pigment found within splenic macrophages (hemosiderophages). In all mice in this study, there was a moderate amount of splenic hemosiderophages, most likely representing normal physiologic extramedullary hematopoiesis in murine spleens. However, the amount and appearance of the hemosiderin (dense, golden-brown, variably-sized, coarse intracytoplasmic pigment granules on H&E) appeared to greatly overwhelm the inherent very fine, black, granular appearance of the PEG-R-Si-Au-NPs on H&E sections. Prussian-blue staining did not alleviate this problem, since the intense dark blue nature of the positive-staining hemosiderin also overwhelmed the inherent very fine, black, granular appearance of the PEG-R-Si-Au-NPs. In summary, PEG-R-Si-Au-NPs are efficiently removed from the systemic circulation by the RES where they are taken up resident macrophages.

In order to reduce aggregation, the surface charge and coating of nanoparticles can be changed with the addition of PEG (19). In addition, as nanoparticles are likely to be opsonized by serum proteins (i.e. clotting and complement proteins) which tag them for RES clearance, PEGylation has been shown to increase nanoparticle bioavailability by protecting them from opsonization and thereby reducing their interaction and uptake by macrophages (17). However, our results show that PEG-R-Si-Au-NPs with a 5:1 ratio of Mal-PEG_{2000}-OME to Mal-PEG_{5000}-NHS are still efficiently taken up by the RES. This would be ideal for PEG-R-Si-Au-NPs applied into the bowel lumen, since any nanoparticles that do manage to enter the systemic circulation will be rapidly removed by the RES thereby limiting the potential for them to cause toxicity. Future alternative clinical applications that require *IV* administration of PEG-R-Si-Au-NPs would therefore need a different PEG ratio tailored to prolong their bioavailability.

Despite there being no pigment within hepatocytes at any time after *IV* PEG-R-Si-Au-NP administration, a mild degree of hepatocyte apoptosis was seen in all animals 24-hours after injection with PEG-R-Si-Au-NPs. Interestingly, the apoptosis also coincided with the time when the most pigment, and thus PEG-R-Si-Au-NPs, was seen in macrophages. We therefore hypothesize, and offer indirect support, for a potential mechanism by which macrophages can signal neighboring hepatocytes to undergo apoptosis. As PEG-R-Si-Au-NPs are known to cause an increase in free radical formation (13), one possibility is that they induce an increase in cellular oxidative stress within hepatocytes and macrophages. Our data support this and show an increase in the gene-expression of phase-2 antioxidant

enzymes within the liver. Despite an early increase in glutathione peroxidase and hemoxygenase transcription, the initial antioxidant defenses were probably overwhelmed since hepatocytes still increased their Bax:Bcl-2 ratio, which is known to cause activation of cellular pro-apoptotic mechanisms (20). As a result, expression of inflammatory (TNF-α and IL-6) and apoptotic (caspase) genes was increased by 24 hours, which resulted in hepatocyte apoptosis, as seen histologically and circumstantially confirmed by TUNEL assay. However, no apoptosis was seen by 1 week after injection, which can be explained by an increase in gene expression of catalase and superoxide dismutase, both of which inhibit apoptosis by removing superoxide free radicals and hydrogen peroxide respectively (21). Taken together, these results suggest that the liver initiates a controlled apoptotic response to PEG-R-Si-Au-NPs in the acute phase after exposure. Given the regenerative capacity of the liver and its role as a filter within the RES, this acute phase response seems intuitive if the liver is to eliminate foreign material that it extracts from the circulation in a controlled and regulated manner.

Following *PR* administration, PEG-R-Si-Au-NPs were cleared from the bowel after 5 min with no nanoparticles detected systemically within any organ for the duration of the study. In a single female mouse, there was a trace concentration of gold within the blood at 5 min and 2 hours after exposure. This was probably due to a slightly traumatic colonic catheterization that could have resulted in a small breach in the integrity of the colonic epithelium thereby allowing PEG-R-Si-Au-NPs to enter the circulation. Another possibility may have been increased absorption of nanoparticles by colonic macrophages within the gut-associated lymphoid tissue in this animal. The results therefore suggest that non-targeted PEG-R-Si-Au-NPs remain in the bowel lumen, do not cross the bowel-wall, and are effectively eliminated from animals by defecation.

It is increasingly being appreciated that the detection of any single molecular biomarker will not provide clinicians with enough confidence to diagnose and characterize a disease process. Instead, multiple biomarkers will need to be detected in order to confidently diagnose and detect diseases with high specificity and sensitivity, especially with complex diseases such as cancer that arise from many accumulated mutations. Hence the ability to detect multiple targets, simultaneously, *in vivo*, has been the focus of many molecular imaging strategies. Although nanoscale based platforms have been created to detect multiple molecular targets for *in vitro* applications, very few nanoparticles have been created for *in vivo* multiplex imaging (22–24). Fluorescent nanoprobes, quantum dots and R-Si-Au-NPs are the predominant molecular imaging probes being assessed for *in vivo* multiplex imaging. However, both fluorescent nanoprobes and quantum dots share similar limitations including autofluorescence, susceptibility to photobleaching and relatively broad emission spectra which limit their ability to co-localize multiple nanoprobes. Under certain condition, quantum dots have also been shown to be cytotoxic thereby significantly limiting their application in humans (25). In contrast, R-Si-Au-NPs do not suffer from these limitations and can be detected at picomolar concentrations, which is almost 1000 fold more sensitive compared to imaging with quantum dots (12). In addition, 5 spectrally-unique R-Si-Au-NPs can be identified and spectrally separated *in vivo* thereby supporting their continued development for future translation into humans as a molecular imaging probe to be used with Raman spectroscopy. Although long-term studies are also still necessary to examine the fate of PEG-R-Si-Au-NPs in the body, our encouraging results show that PEG-R-Si-Au-NPs are not toxic in the short term and thus support the continued development of this nanoparticle as a molecular imaging probe. In particular, further work can now be undertaken to target these nanoparticles to molecular biomarkers up-regulated in specific diseases.

One of the limitations of any optical imaging technique, including Raman spectroscopy, is limited depth penetration. Hence, we are applying Raman spectroscopy with targeted-PEG-R-Si-Au-NPs to detect diseases within hollow viscera, thereby allowing a Raman laser to be in close proximity to the tissue being interrogated. Hence, a uniquely designed Raman-endoscope is currently being developed with a vision that targeted-PEG-R-Si-Au-NPs can be applied into the bowel lumen during routine colonoscopy to detect colon cancer. This will provide clinicians with a powerful biologically driven imaging technique and an accompanying specifically designed device to detect early colon cancer, including flat lesions (26), in real time. The advantage of initially focusing on colon cancer is its high prevalence. In addition, any potential long term effects of PEG-R-Si-Au-NPs will be minimized since nanoparticles are expected to be excreted from the body following the procedure. Currently, we are identifying molecular biomarkers which are specifically up regulated in human colon cancer. One example is the epidermal growth factor receptor (EGFR) (27, 28) and another strategy relies on a heptapeptide sequence, VRPMPLQ, which has been shown to preferentially bind to pre-malignant colon cancer tissue with high affinity (29). Hence, we are in the process of optimizing the labeling of PEG-R-Si-Au-NPs either with an affibody which binds specifically to the EGFR or with the heptapeptide sequence, VRPMPLQ. Once we have proven the ability of targeted-PEG-R-Si-Au-NP to bind to human dysplastic colonic tissue with a high sensitivity and specificity, further toxicity studies will need to be undertaken to examine if these functionalized nanoparticles are processed differently by living animals. This is especially important since recent studies have shown that functionalized or coupled nanoparticles are taken up by colon cancer cells significantly more readily when compared to uncoupled nanoparticles (30). However, pilot studies using a prototype tumor-targeted-nanoparticle construct (e.g. VRPMPLQ-PEG-R-Si-Au-NP) have been undertaken in collaboration with the Nanocharacterization Lab at the National Cancer Institute (See supplementary discussion). The preliminary results are encouraging and show that in a small cohort of mice, peptide-functionalized-PEG-R-Si-Au-NPs do not get into the blood after colorectal administration; highly supportive of a lack of systemic toxicity of these functionalized nanoparticles. Other potential applications for these nanoparticles include the detection of all other cancers which can be reached endoscopically such as oesophageal, stomach, small bowel, bronchial and bladder cancer. As therapeutic drugs can also be conjugated to PEG-R-Si-Au-NPs, this will allow the development of an integrated diagnostic and therapeutic nanoparticle in the future.

Supplementary discussions

Over 2 weeks, the level of gold within the liver slowly declined after *IV* PEG-R-Si-Au-NP, as determined by ICP-MS, suggesting that some PEG-R-Si-Au-NPs are probably being removed from the animal via heptobillary excretion. However, as PEG-R-AuNPs do not cross the bowel-wall and are not absorbed by intestinal cells, the only way to confirm this would have been to collect, separate and analyze all the feces and urine produced by all *IV* injected mice over the two weeks. Although we did collect samples of feces and, when possible, urine for analysis by ICP-MS, this is only a snapshot representation of a dynamic excretory process and hence it is not surprising that no gold was detected in these samples. Interestingly, there was a peak in gold concentration within the spleen at 24 hours suggesting that up to this time, PEG-R-Si-Au-NPs were still being redistributed within animals. In a single male animal, a small concentration of gold (1.31 ppm/g) was detected in a lung sample at 5 min. In this case, it is likely that the some of the PEG-R-Si-Au-NPs in this animal bypassed the macrophages in the liver and spleen but were subsequently removed from the circulation by macrophages within the lung, which is another organ of the RES.

A mild degree of mitosis was also seen in male and female mice at 24 hours and 1 week following both *IV* saline and PEG-R-Si-Au-NP administration. This phenomenon has been previously observed and can be attributed to stretch-induced localized proliferation of hepatocytes due to swelling of liver sinusoids after a tail vein injection (31). The stretching of cells increases DNA synthesis and cell proliferation by activating tyrosine kinases and protein kinase C (32). In addition, the release of other growth factors and stimuli from the neighboring cells which have undergone apoptosis may also contribute to the local mitotic response (31).

Initial pilot studies using a prototype tumor targeted nanoparticle construct have been undertaken in collaboration with the Nanocharacterization Lab (NCL) at the National Cancer Institute (NCI). Here, PEG-R-Si-Au-NP were conjugated with the heptapeptide sequence, VRPMPLQ, using simple amine chemistry. In 5 male and 5 female mice, 200 μl of 0.8nM VRPMPLQ-PEG-R-Si-Au-NP (=9.6×10^{10} tumor targeted nanoparticles) were rectally administered. All mice were sacrificed 3 days after PR VRPMPLQ-PEG-R-Si-Au-NP administration and gastrointestinal penetration analysis commenced. Necropsy included (i) ICP analysis of sentinel organs (liver and colon), feces and urine, (ii) detailed histopathology of all major tissues and (iii) hematology and clinical chemistry panels. The results show that in all experimental mice, no nanoparticles were detected in the systemic circulation 3 days after PR VRPMPLQ-PEG-R-Si-Au-NP administration. In addition, ICP analysis only revealed gold content within the feces with undetectable amounts of gold in sentinel organs (liver and colon). Histopathology revealed healthy tissues in all mice with no biological effects of VRPMPLQ-PEG-R-Si-Au-NPs. Comprehensive hematology and clinical chemistry panels were all normal. As no VRPMPLQ-PEG-R-Si-Au-NPs entered into blood, it is therefore unlikely that these nanoparticles cause any systemic toxicity. However, more detailed studies may be needed to study different types of targeted particles for any potential toxicity.

MATERIALS AND METHODS

Animals

All animal experiments were conducted in compliance with the relevant guidelines and regulations approved by the Stanford Administrative Panel on Laboratory Animal Care (APLAC). A total of one hundred and twenty (120) 5 week-old male and female FVB mice were obtained from a pathogen-free colony (Charles Rivers Laboratory). Male and female FVB mice were chosen to assess the response to PEG-R-Si-Au-NPs because they have fully competent immune systems. Mice were housed in same-sex groups with three animals per cage. Water and food were available to all mice *ad libitum*. The environmental conditions were carefully monitored and maintained within an acceptable range throughout the study (temperature 66±2°F; relative humidity 39±1%; 12-h light/dark cycle). All animals were quarantined for 7-days prior to the commencement of any experimental studies.

Nanoparticle characteristics

The R-Si-Au-NPs were obtained from Oxonica Materials Inc (Mountain View, CA) and consisted of a 60 nm gold core, a Raman organic molecule and a 30 nm silica shell, making the entire nanoparticle on the order of 120 nm in diameter (Fig. 1). This arrangement dramatically increases the incident electromagnetic field of the Raman active organic molecule, thereby significantly amplifying its Raman signal intensity. Recent studies by our group have shown that these R-Si-Au-NPs have ultra-high sensitivity and can be detected at picomolar concentrations *in vivo* (6). In addition, as the bound Raman organic molecule can be altered between different nanoparticles, different R-Si-Au-NPs are therefore able to provide different spectral signatures. Accordingly, we have shown the ability of Raman

spectroscopy to separate the spectral signature of 5 different R-Si-Au-NPs in a living mouse following *IV* injection (12). The particular lot used in this study was the S440 batch which consists of a unique Raman material layer (Trans-1,2-Bis(4-pyridyl)-ethylene) and its associated spectrum which is detailed in previous work (6). The R-Si-Au-NPs were PEGylated, but not further functionalized (e.g. using targeting peptides), in order to study the core nanoparticle. Two different sized PEG molecules, Mal-PEG_{2000}-OME and Mal-PEG_{5000}-NHS, were added to the surface of the R-Si-Au-NP in a 5:1 ratio, respectively. The smaller Mal-PEG_{2000}-OME was added to improve nanoparticle biocompatibility while the larger Mal-PEG_{5000}-NHS was added to provide a functional group for potential ligand attachment. Both surface-PEG chains were added to the surface of these nanoparticles in a two-step process. Initially, thiol groups were introduced into the silica shell of the nanoparticle using 3-mercaptopropyltrimethoxysilane. This was followed by conjugation with malemide activated mPEGs, where the malemide group reacted with the thiol group on the nanoparticle surface at neutral pH. In order to ensure consistency between the experiments, all PEG-R-Si-Au-NPs were created at the same time from the same batch of stock nanoparticles received from Oxonica Materials Inc. All nanoparticles were stored at 4°C between experiments.

Experimental Protocol

To assess the effect of *IV* and *PR* R-Si-Au-NP administration, mice were randomly allocated into two experimental groups each containing sixty mice with an equal male-to-female sex ratio (Fig. S4). In the *IV* group, three male and three female mice for each time point were given a 200 μl IV injection (via the tail vein) of either sterile saline or PEG-R-Si-Au-NPs. Since the concentration of the stock solution of nanoparticles provided by Oxonica Materials Inc. was 0.8nM, using Avogadro's Constant (6.022×1023 elementary entities per mole of substance) we determined that there were 481760000 PEG-R-Si-Au-NP per μl of stock solution. From this information, we were able to achieve a final concentrations of 9.6×10^{10} nanoparticles in 200 μl of saline. Mice in the *PR* group were fasted overnight in special metabolic cages with wire floors which allowed any feces produced to drop into a waste container. This prevented mice from having access to their feces during the fasting period thereby ensuring their large bowel was completely evacuated and prepared prior to any PEG-R-Si-Au-NP administration. The following day, three male and three female mice for each time point were given a 200 μl *PR* injection of either sterile saline or PEG-R-Si-Au-NPs using a 24-gauge angiocatheter. All mice were euthanized by carbon dioxide asphyxiation at specific time points: 5 min, 2 hours, 24 hours, 1 week and 2 weeks post PEG-R-Si-Au-NP administration (Fig. S4).

Mice which were euthanized at 2 weeks post PEG-R-Si-Au-NP administration were carefully monitored throughout the study. For each mouse, their physical appearance (fur, eyes, mucous membranes, secretions, stool, gait, posture, breathing pattern), behavior (gait, posture, stereotypes, vocalizations) and interactions towards other animals were assessed and recorded daily. The body weight and cardiovascular status (ECG measurements using subcutaneous electrodes and blood pressure and heart rate measurements using a tail vein cuff device (Coda 6, Kent Scientific Corporation)) for each mouse were also recorded weekly. In addition, 200 μl of blood was collected from each mouse via retro-orbital bleeding through a heparin coated glass tube 1 week prior to PEG-R-Si-Au-NP administration to determine the baseline complete blood count (CBC), chemistry and electrolyte panels (Veterinary Service Centre of the Department of Comparative Medicine at Stanford University). Since APLAC protocol restricted subsequent blood withdrawal to <200 μl for each animal, only CBC and chemistry panels were determined at the beginning of the second week following PEG-R-Si-Au-NP administration. Blood samples for electrolytes were subsequently taken at the end of the second week immediately after

euthanasia via cardiopuncture. However, it was not possible to analyze chemistry panels from samples collected via cardiopuncture due to the well described phenomenon of muscle tissue contamination encountered with this particular blood collection procedure (33). Prior to any blood sample collection all mice were fasted overnight.

Pathologic Evaluation

A complete *post mortem* examination was performed on each mouse at all time points, and examined for gross changes. Samples of all major organs and tissues were collected and fixed in neutral-buffered 10% formalin for 48 hours. Fixed samples of liver, spleen, colon, small intestine, heart, kidneys, lungs, brain, and gonads were then routinely processed and stained with hematoxylin and eosin (H&E; Histotec Laboratories, Hayward, CA) for light microscopy. Histopathological examination was performed by a veterinary pathologist blinded to other findings. Histopathologic diagnosis was performed according to the Standardized System of Nomenclature and Diagnostic Criteria (SSNDC).

Immunohistochemistry

To assess the co-localization of PEG-R-Si-Au-NPs and macrophages, paraffin-embedded, formalin-fixed liver and spleen tissues from a representative male and female administered with PEG-R-Si-Au-NP from each time point were chosen and immunostained with a rat anti-mouse purified monoclonal antibody against the F4/80 macrophage specific membrane antigen (AbD Serotec). Tissues were cut 4 mm thick by a microtome and stained using a StreptAvidin-HRP immunoperoxidase method. Endogenous peroxidase activity was inhibited by 3 % hydrogen peroxide for 10 min followed by enzyme digestion in trypsin for 15 min at room temperature. Sections were then incubated for 2 hours with the primary F4/80 antibody. A saline treated animal was used as a positive control and an animal which had both received PEG-R-Si-Au-NPs and been incubated without the primary antibody was used as a negative control. After three washes with PBS for 5 min each, the sections were incubated for 30 min with a goat-anti rat-biotinylated secondary antibody for 30 min. StreptAvidin-HRP was applied for 30 min and reacted with diaminobenzidine hydrochloride and counterstained with hematoxylin. Immunostained sections were then evaluated by a veterinary pathologist.

Despite two separate attempts by independent laboratories, control and experimental tissues did not react with the monoclonal antibody against the F4/80 macrophage specific antigen. The failure of the F4/80 antibody to immunoreact with the macrophages in the tissues of our control and experimental mice could be due to significant alterations in the epitope structure of the F4/80 macrophage antigen (e.g, inappropriate fixation or inherent differences in the F4/80 epitope in this group of mice), incorrect methodology (e.g., failure to replicate the manufacturer's instructions), or issues with the antibody used itself (e.g., incorrect generation of the appropriate antibody, incorrect storage/transport of the antibody). However, we feel that incorrect methodology is unlikely since manufacturer's instructions were followed originally (with subsequent attempts to make the antibody "work" deviating from manufacturer's instructions based on each laboratory's experience).

TUNEL Assay

To assess the co-localization of PEG-R-Si-Au-NPs and apoptotic cells, paraffin-embedded, formalin-fixed liver and spleen tissues from a representative male and female animal from each time point which had received PEG-R-Si-Au-NPs were chosen and stained with an *in situ* terminal deoxynucleotidyl transferase-mediated dUTP nick end-labeling (TUNEL) kit (Millipore), following the manufacturer's protocol for paraffin sections. Using a light microscope, the number of positively stained cells per 100 cells was counted by a veterinary pathologist.

Scanning Transmission Electron Microscopy

During gross pathologic examination, samples of liver, spleen, colon, small intestine, kidneys, lungs, brain and gonads (measuring approximately $1mm^3$) were collected in a 2:1:1 solution of 0.2 M sodium cacodylate buffer: 10 % glutaraldehyde: 8 % paraformaldehye (EMSdiasum). Samples were then stored at 4 °C before being stained *en bloc* with osmium tetroxide and uranyl acetate. Samples were then dehydrated in increasing concentrations of ethanol, followed by further dehydration using propylene oxide before being embedded in Embed 812 epoxy resin (EMSdiasum). Thin sections (150 nm) of each embedded tissue were cut using a Leica Ultracut S microtome and placed on 200 mesh bare copper grids. Sections were then examined using a Tecnai F20 (FEI) transmission electron microscope operating at 120kV. Scanning transmission electron microscopy (STEM) was utilized to analyze 12500 μm^3 of tissue from each sample in order to determine the intracellular location of PEG-R-SI-Au-NPs. Tissue sections (150 nm) were also placed on a formvar coated 1x2 mm slot grid to collect a series of images at different tilt angles to perform a tilt series 3D reconstruction. Dark field STEM images were collected at 1 degree intervals from −40 °C to +25 °C. Tilt series alignment and reconstruction was performed with assistance from FEI Company using the Inspect 3D reconstruction Package.

Inductively coupled plasma-mass spectrometry

During gross pathologic examination, samples of liver, spleen, colon, small intestine, kidneys, lungs, brain and gonads (measuring approximately 1 mm^3) were collected to determine concentrations of gold in each of these tissues by ICP-MS analysis. Samples were prepared by microwave-assisted acid digestion to dissolve the gold core for ICP analysis using a mixture of trace metal grade 70 % nitric acid (HNO_3; Fisher Sci), 37 % hydrochloric acid (HCl; Fisher Sci), and 48 % hydrofluoric acid (HF; Fisher Sci). All samples were digested with hydrofluoric acid to dissolve the outer silica shell of the PEG-R-Si-Au-NP, thereby freeing the elemental gold core for measurement by ICP-MS (34). Samples were then air-dried, heated and re-suspended in freshly prepared aqua regia diluted with double distilled water to 5x volume. ICP-MS was undertaken using a JA IRIS Advantage/1000 Radial ICAP Spectrometer which was calibrated using a 2 ppm [Au] high standard and a 1 ppm [Au] QC standard (Gold ICP standard; 1ml = 1mg Au (1,000ppm Au), Ricca Chemical, Fisher Scientific, PAU 1KH100) in dilute aqua regia matrix. Based on pilot experiments, the detection limit for the detection of gold was set at 0.019 ppm [Au]. The reproducibility of the spectrometer was determined by measuring a series of different [Au] standards in triplicate: 1.0 ppm [Au] was measured to an accuracy of 0.9914±0.0063, 0.1 ppm [Au] was measured to an accuracy of 0.1003±0.0025, 0.01 ppm [Au] was measured to an accuracy of 0.0103±0.0010.

Assessment of antioxidant enzyme and inflammatory gene expression using q-RT-PCR

During gross pathologic examination, a sample of liver was collected and stored at −80 °C. The change in gene expression in liver samples from animals which had been administered *IV* PEG-R-Si-Au-NPs were evaluated and compared with control animals which had received *IV* saline according to methods described previously(35). Total ribonucleic acid (RNA) was extracted from sonicated liver tissue using RNeasy Plus Mini Kit (Qiagen) which contained gDNA eliminator spin columns to effectively remove genomic DNA. The RNA concentration in each sample was then calculated using the Qbit system (Invitrogen). Using 1 μg of RNA, cDNA was synthesized using reverse transcription (RT) by incubating samples at 25 °C for 5 min followed by 42 °C for 45 min with qScript cDNA Supermix (Quanta Biosciences) which contained buffer, dNTPs, $MgCl_2$, random primers, RNase inhibitor and Reverse Transcriptase. Quantitative reverse transcription polymerase chain reaction (q-RT-PCR) was then undertaken using the Realplex Mastercycler machine

(Eppendorf) with PerfeCTa SYBR Green FastMix which contained AccuFast Taq DNA polymerase (Quanta Biosciences). All samples were run in triplicate in a 20 μL reaction volume using cDNA of 100 ng RNA equivalent with an initial pre-heating phase of 95 °C for 2 min followed by 60 cycles consisting of 95 °C for 30 sec, 55 °C for 30 sec and 68 °C for 30 sec. Melting curve analysis was performed for each reaction to exclude nonspecific PCR side products. The primer sequences for antioxidant enzyme genes (catalase, superoxide dismutase, hemoxygenase and glutathione peroxidase) and inflammatory genes (Bax, Bcl-2, Capase-3, IL-6 and TNF-α) along with the internal control (β-actin) are shown in Table S4. As the RNA extraction for some liver samples did not generate sufficient quantities of RNA to run q-RT-PCR, male and female samples for the PEG-R-Si-Au-NP and control groups were analyzed together at each time point. Statistical analysis using a two-way RM ANOVA was therefore performed comparing the effect of time (5 min, 2 hours, 24 hours, 1 week and 2 weeks) and treatment (*intravenous* or *per rectum* saline *vs.* PEG-R-Si-Au-NP).

Statistical Analysis

All quantitative variables are expressed as mean ± standard error of the mean (SEM). When possible, a three-way RM ANOVA was performed comparing the effect of time (5 min, 2 hours, 24 hours, 1 week and 2 weeks), treatment (*intravenous or per rectum* saline *vs.* PEG-R-Si-Au-NP) and sex (male *vs.* female). Where a significant effect of time, group or sex was indicated, the *post hoc* Student-Newman-Keuls test was used to isolate the statistical differences. For all comparisons, statistical significance was accepted when $P < 0.05$.

Supplementary Material

Refer to Web version on PubMed Central for supplementary material.

Acknowledgments

We thank Ian Walton at Oxonica Inc. for helpful advice. We also thank Dr. Anil Patri and colleagues at the Nanocharacterization lab (NCL), National Cancer Institute at Frederick.

Funding: Supported by the NCI Center for Cancer Natotechnology Excellence (CCNE) U54 CA119367 (S.S.G.), NCI Network for Translational Research (NTR): Optical Imaging in Multimodality Platforms (S.S.G.), the NCI In vivo cellular and Molecular Imaging Centers (ICMIC) P50 CA114747 (S.S.G.), the Canary Foundation (S.S.G.), the American Cancer Society (A.S.T.), the European Association for Cancer Research (A.S.T.), and the PEEL Medical Research Trust (A.S.T.), and NIHR Cambridge Biomedical Research Centre (A.S.T. and T.F.M.).

References

1. Blasberg RG. Molecular imaging and cancer. Mol Cancer Ther. 2003; 2:335–343. [PubMed: 12657729]
2. Gambhir SS. Molecular imaging of cancer with positron emission tomography. Nat Rev Cancer. 2002; 2:683–693. [PubMed: 12209157]
3. Massoud TF, Gambhir SS. Molecular imaging in living subjects: seeing fundamental biological processes in a new light. Genes Dev. 2003; 17:545–580. [PubMed: 12629038]
4. Pysz MA, Gambhir SS, Willmann JK. Molecular imaging: current status and emerging strategies. Clin Radiol. 65:500–516. [PubMed: 20541650]
5. Lee S, Kim S, Choo J, Shin SY, Lee YH, Choi HY, Ha S, Kang K, Oh CH. Biological imaging of HEK293 cells expressing PLCgamma1 using surface-enhanced Raman microscopy. Anal Chem. 2007; 79:916–922. [PubMed: 17263316]
6. Keren S, Zavaleta C, Cheng Z, de la Zerda A, Gheysens O, Gambhir SS. Noninvasive molecular imaging of small living subjects using Raman spectroscopy. Proc Natl Acad Sci U S A. 2008; 105:5844–5849. [PubMed: 18378895]

7. Hanlon EB, Manoharan R, Koo TW, Shafer KE, Motz JT, Fitzmaurice M, Kramer JR, Itzkan I, Dasari RR, Feld MS. Prospects for in vivo Raman spectroscopy. Phys Med Biol. 2000; 45:R1–59. [PubMed: 10701500]
8. Kamemoto LE, Misra AK, Sharma SK, Goodman MT, Luk H, Dykes AC, Acosta T. Near-infrared micro-Raman spectroscopy for in vitro detection of cervical cancer. Appl Spectrosc. 64:255–261. [PubMed: 20223058]
9. de Carvalho LF, Bitar RA, Arisawa EA, Brandao AA, Honorio KM, Cabral LA, Martin AA, Martinho Hda S, Almeida JD. Spectral region optimization for Raman-based optical biopsy of inflammatory lesions. Photomed Laser Surg. 28(Suppl 1):S111–117. [PubMed: 20690839]
10. Huang Z, Bergholt MS, Zheng W, Lin K, Ho KY, Teh M, Yeoh KG. In vivo early diagnosis of gastric dysplasia using narrow-band image-guided Raman endoscopy. J Biomed Opt. 2010; 15:037017. [PubMed: 20615046]
11. Banholzer MJ, Millstone JE, Qin L, Mirkin CA. Rationally designed nanostructures for surface-enhanced Raman spectroscopy. Chem Soc Rev. 2008; 37:885–897. [PubMed: 18443674]
12. Zavaleta CL, Smith BR, Walton I, Doering W, Davis G, Shojaei B, Natan MJ, Gambhir SS. Multiplexed imaging of surface enhanced Raman scattering nanotags in living mice using noninvasive Raman spectroscopy. Proc Natl Acad Sci U S A. 2009; 106:13511–13516. [PubMed: 19666578]
13. Thakor AS, Paulmurugan R, Kempen P, Zavaleta C, Sinclair R, Massoud TF, Gambhir SS. Oxidative stress mediates the effects of Raman-active gold nanoparticles in human cells. Small. 2011; 7:126–136. [PubMed: 21104804]
14. Brandenberger C, Rothen-Rutishauser B, Muhlfeld C, Schmid O, Ferron GA, Maier KL, Gehr P, Lenz AG. Effects and uptake of gold nanoparticles deposited at the air-liquid interface of a human epithelial airway model. Toxicol Appl Pharmacol. 242:56–65. [PubMed: 19796648]
15. Pan Y, Neuss S, Leifert A, Fischler M, Wen F, Simon U, Schmid G, Brandau W, Jahnen-Dechent W. Size-dependent cytotoxicity of gold nanoparticles. Small. 2007; 3:1941–1949. [PubMed: 17963284]
16. Goodman CM, McCusker CD, Yilmaz T, Rotello VM. Toxicity of gold nanoparticles functionalized with cationic and anionic side chains. Bioconjug Chem. 2004; 15:897–900. [PubMed: 15264879]
17. Schipper ML, Iyer G, Koh AL, Cheng Z, Ebenstein Y, Aharoni A, Keren S, Bentolila LA, Li J, Rao J, Chen X, Banin U, Wu AM, Sinclair R, Weiss S, Gambhir SS. Particle size, surface coating, and PEGylation influence the biodistribution of quantum dots in living mice. Small. 2009; 5:126–134. [PubMed: 19051182]
18. Cho M, Cho WS, Choi M, Kim SJ, Han BS, Kim SH, Kim HO, Sheen YY, Jeong J. The impact of size on tissue distribution and elimination by single intravenous injection of silica nanoparticles. Toxicol Lett. 2009; 189:177–183. [PubMed: 19397964]
19. Otsuka H, Nagasaki Y, Kataoka K. PEGylated nanoparticles for biological and pharmaceutical applications. Adv Drug Deliv Rev. 2003; 55:403–419. [PubMed: 12628324]
20. Korsmeyer SJ, Shutter JR, Veis DJ, Merry DE, Oltvai ZN. Bcl-2/Bax: a rheostat that regulates an anti-oxidant pathway and cell death. Semin Cancer Biol. 1993; 4:327–332. [PubMed: 8142617]
21. Haddad JJ. Redox and oxidant-mediated regulation of apoptosis signaling pathways: immuno-pharmaco-redox conception of oxidative siege versus cell death commitment. Int Immunopharmacol. 2004; 4:475–493. [PubMed: 15099526]
22. Xing Y, Chaudry Q, Shen C, Kong KY, Zhau HE, Chung LW, Petros JA, O'Regan RM, Yezhelyev MV, Simons JW, Wang MD, Nie S. Bioconjugated quantum dots for multiplexed and quantitative immunohistochemistry. Nat Protoc. 2007; 2:1152–1165. [PubMed: 17546006]
23. Chan WC, Maxwell DJ, Gao X, Bailey RE, Han M, Nie S. Luminescent quantum dots for multiplexed biological detection and imaging. Curr Opin Biotechnol. 2002; 13:40–46. [PubMed: 11849956]
24. Sun L, Yu C, Irudayaraj J. Surface-enhanced Raman scattering based nonfluorescent probe for multiplex DNA detection. Anal Chem. 2007; 79:3981–3988. [PubMed: 17465531]
25. Medintz IL, Mattoussi H, Clapp AR. Potential clinical applications of quantum dots. Int J Nanomedicine. 2008; 3:151–167. [PubMed: 18686776]

26. Wallace MB, Kiesslich R. Advances in endoscopic imaging of colorectal neoplasia. Gastroenterology. 138:2140–2150. [PubMed: 20420951]
27. Hsiung PL, Wang T. In vivo biomarkers for targeting colorectal neoplasms. Cancer Biomark. 2008; 4:329–340. [PubMed: 19126961]
28. Radinsky R, Risin S, Fan D, Dong Z, Bielenberg D, Bucana CD, Fidler IJ. Level and function of epidermal growth factor receptor predict the metastatic potential of human colon carcinoma cells. Clin Cancer Res. 1995; 1:19–31. [PubMed: 9815883]
29. Hsiung PL, Hardy J, Friedland S, Soetikno R, Du CB, Wu AP, Sahbaie P, Crawford JM, Lowe AW, Contag CH, Wang TD. Detection of colonic dysplasia in vivo using a targeted heptapeptide and confocal microendoscopy. Nat Med. 2008; 14:454–458. [PubMed: 18345013]
30. Jain A, Jain SK. In vitro and cell uptake studies for targeting of ligand anchored nanoparticles for colon tumors. Eur J Pharm Sci. 2008; 35:404–416. [PubMed: 18824095]
31. Budker VG, Subbotin VM, Budker T, Sebestyen MG, Zhang G, Wolff JA. Mechanism of plasmid delivery by hydrodynamic tail vein injection. II. Morphological studies. J Gene Med. 2006; 8:874–888. [PubMed: 16718734]
32. Yamamoto H, Teramoto H, Uetani K, Igawa K, Shimizu E. Stretch induces a growth factor in alveolar cells via protein kinase. Respir Physiol. 2001; 127:105–111. [PubMed: 11504583]
33. Wallace Hayes, A. I. Informa Healthcare USA. Principles and methods of toxicology. 5. New York: 2008.
34. Makishima A, Tanaka R, Nakamura E. Precise elemental and isotopic analyses in silicate samples employing ICP-MS: application of hydrofluoric acid solution and analytical techniques. Anal Sci. 2009; 25:1181–1187. [PubMed: 19822960]
35. Pfaffl MW. A new mathematical model for relative quantification in real-time RT-PCR. Nucleic Acids Res. 2001; 29:e45. [PubMed: 11328886]

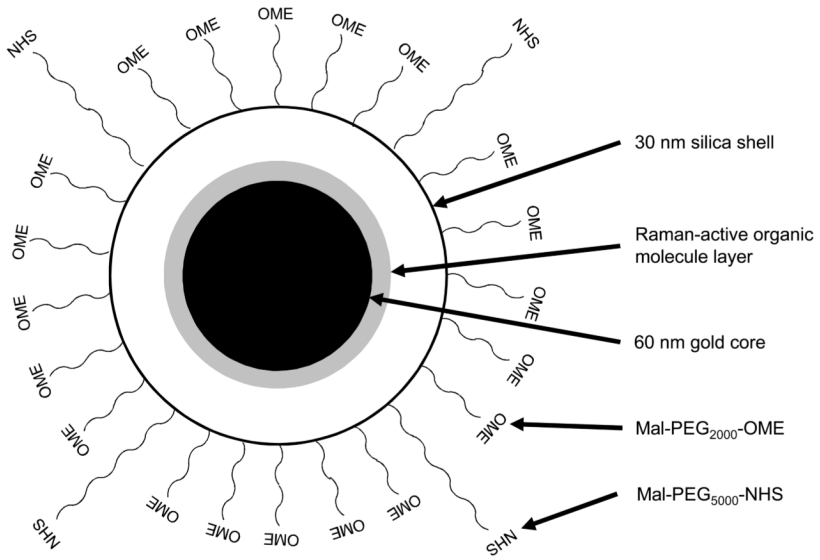

Figure 1. A diagrammatic representation of the PEG-R-Si-Au-NP

PEG=polyethylene glycol; Mal=maleimide; OME=methoxy group; NHS=succinimidyl ester

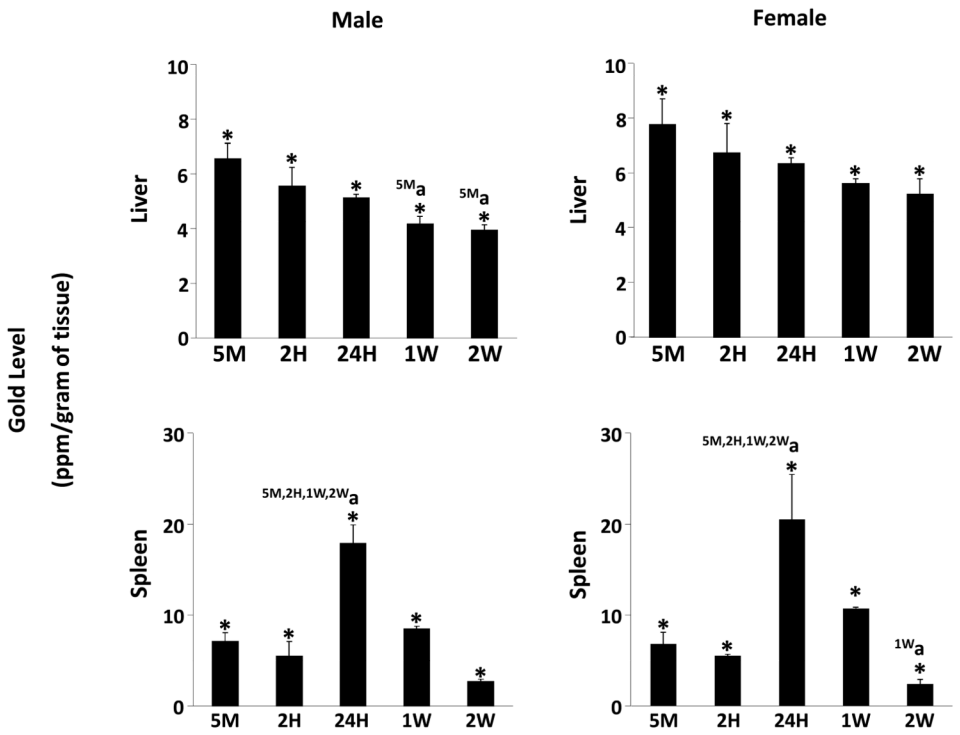

Figure 2. Gold concentrations in the liver and spleen

Bars represent the mean±SEM for the concentration of gold in the liver and spleen as determined by ICP-MS at 5M (5 min), 2H (2 hours), 24H (24 hours), 1W (1 week), 2W (2 weeks) after *IV* PEG-R-Si-Au-NP administration. Significant differences: *P < 0.05, difference from *PR* PEG-R-Si-Au-NP; [a]P < 0.05, difference between time-points within the same group and sex (superscript numbers represent the statistically significant time-point groups); [b]P < 0.05, difference between sexes. Three-way RM ANOVA with *post hoc* Student-Newman-Keuls test

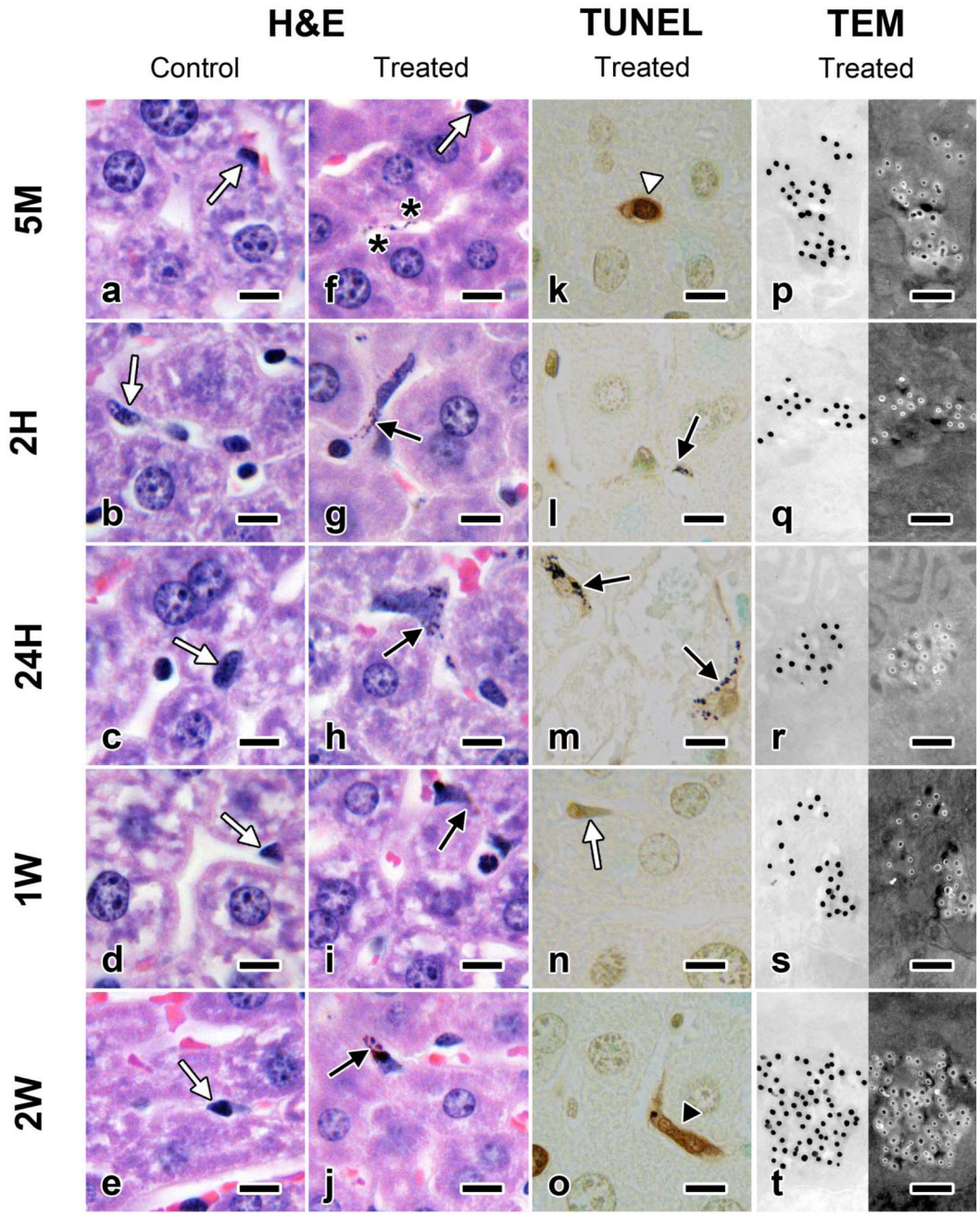

Figure 3. Photomicrographs of liver from male mice after *IV* PEG-R-Si-Au-NP administration. A to E

H&E stained sections of control animals, showing resident macrophages/Kupffer cells (white arrow). 1000X magnification, bar = 10 microns. **F to J**. H&E stained sections of IV PEG-R-Si-Au-NP treated animals, showing resident macrophages/Kupffer cells (white arrow); free, fine, black pigment within sinusoids (black asterisk); and resident macrophages/Kupffer cells with intracytoplasmic, fine, black pigment (black arrow). 1000X magnification, bar = 10 microns. **K to O**. TUNEL stained sections of IV PEG-R-Si-Au-NP treated animals, showing resident macrophages/Kupffer cells (white arrow); resident macrophages/Kupffer cells with intracytoplasmic, fine, black pigment (black arrow);

resident macrophages/Kupffer cells that demonstrated diffuse, brown, intranuclear staining with TUNEL (white arrowhead) and resident macrophages/Kupffer cells with intracytoplasmic, fine, black pigment that demonstrated diffuse, brown, intranuclear staining with TUNEL (black arrowhead). 1000X magnification, bar = 10 microns. **P to T**. Bright (left) and dark (right) field TEM sections of IV R-AuNP treated animals. 59,000X magnification, bar = 200 nanometers.

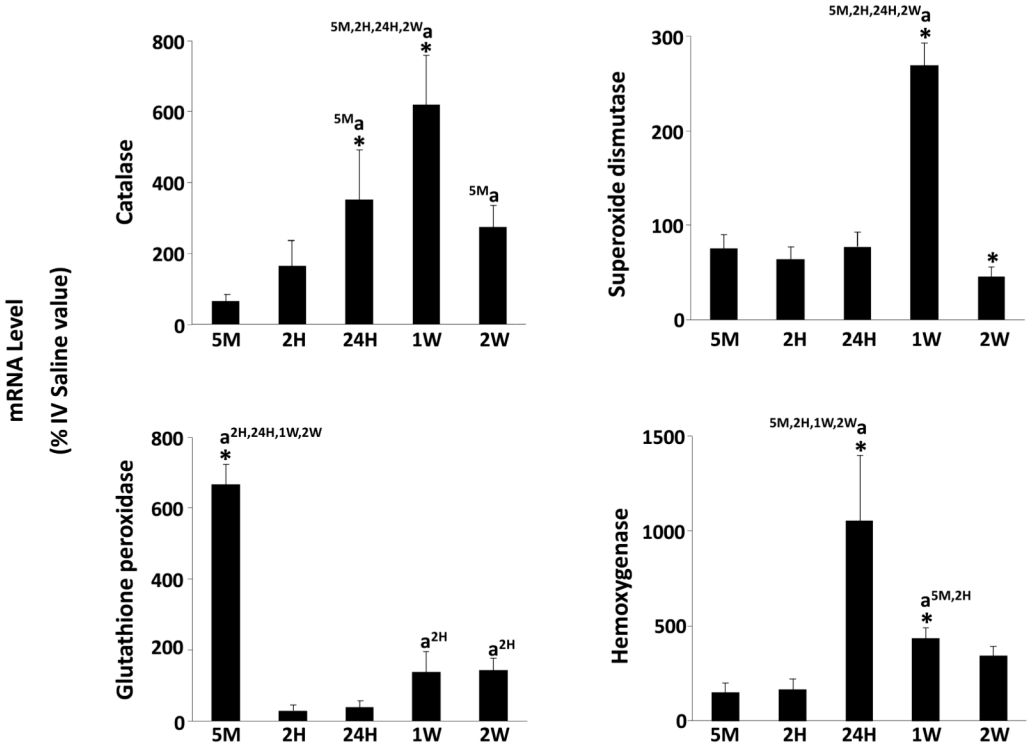

Figure 4. Change in antioxidant enzyme gene expression within the liver tissue after *IV* PEG-R-Si-Au-NP administration

Bars represent the mean±SEM for the fold change in antioxidant enzyme gene expression compared to control cells at 5M (5 min), 2H (2 hours), 24H (24 hours), 1W (1 week), 2W (2 weeks) after *IV* PEG-R-Si-Au-NP administration. Significant differences: *P < 0.05, difference between control animals (*IV* saline) within the same sex; [a]P < 0.05, difference between time-points within the same group and sex (superscript numbers represent the statistically significant time-point groups). Two-way RM ANOVA with *post hoc* Student-Newman-Keuls test

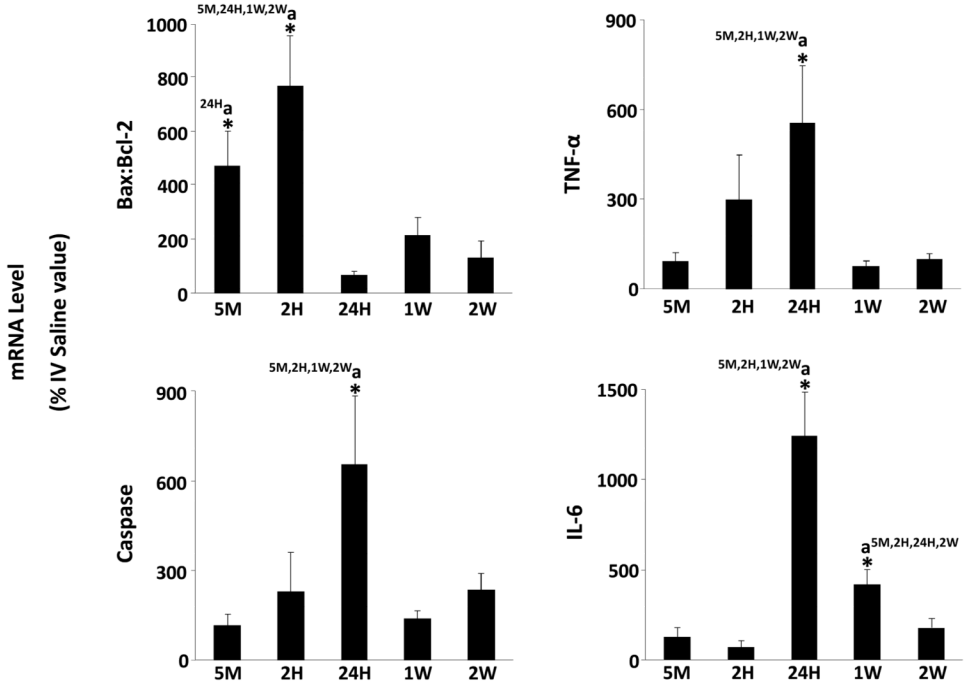

Figure 5. Change in inflammatory gene expression within the liver after *IV* PEG-R-Si-Au-NP administration

Bars represent the mean±SEM for the fold change in inflammatory gene expression compared to control cells at 5M (5 min), 2H (2 hours), 24H (24 hours), 1W (1 week), 2W (2 weeks) following *IV* PEG-R-Si-Au-NP administration. Significant differences: *P < 0.05, difference between control animals (IV saline) within the same sex; [a]P < 0.05, difference between time-points within the same group and sex (superscript numbers represent the statistically significant time-point groups). Two-way RM ANOVA with *post hoc* Student-Newman-Keuls test

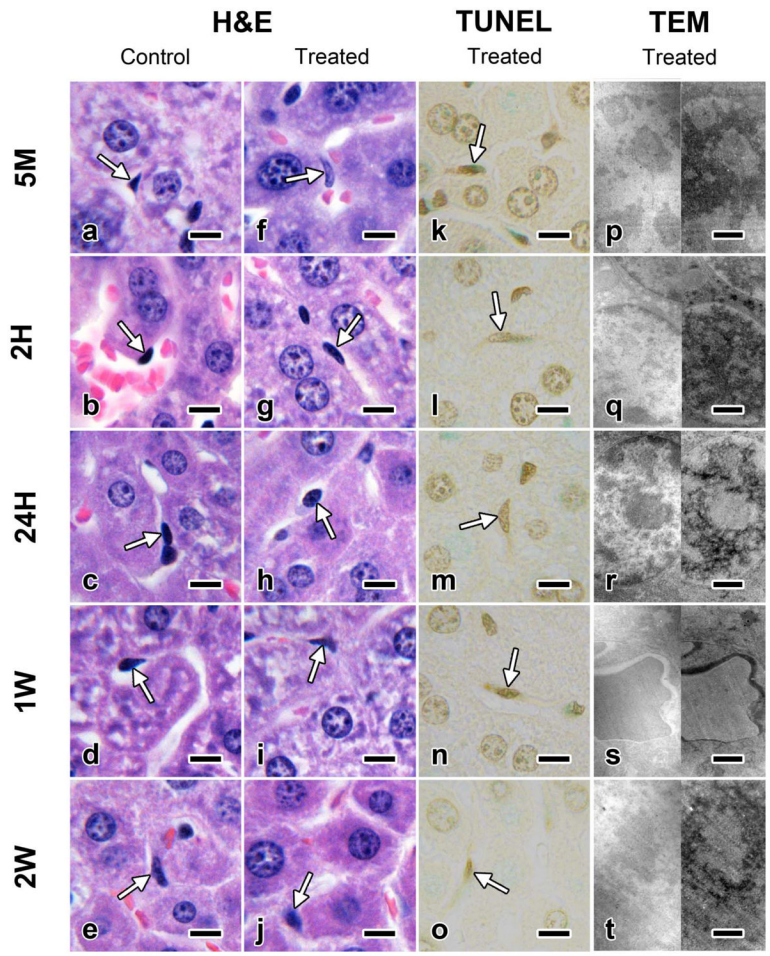

Figure 6. Photomicrographs of liver from male mice after *PR* PEG-R-Si-Au-NP administration. A to E

H&E stained sections of control animals, showing resident macrophages/Kupffer cells (white arrow). 1000X magnification, bar = 10 microns. **F to J.** H&E stained sections of IR R-AuNP treated animals, showing resident macrophages/Kupffer cells (white arrow). 1000X magnification, bar = 10 microns. **K to O.** TUNEL stained sections of IR R-AuNP treated animals, showing resident macrophages/Kupffer cells (white arrow). 1000X magnification, bar = 10 microns. **P to T.** Bright (left) and dark (right) field TEM sections of IR R-AuNP treated animals. 21,000X magnification, bar = 500 nanometers.

Sci Transl Med. Author manuscript; available in PMC 2013 December 26.

Table 1

Histological results from liver tissue after PEG-R-Si-Au-NP administration

The liver from each mouse is represented by a single number corresponding to the severity of the change observed. 0=Normal; 1=Minimal change; 2=Mild change; 3=Moderate change; 4=Severe change

IV Group

		Pigment in Sinusoids		Pigment in Macrophages		Pigment in Hepatocytes		Apoptosis		Necrosis		Mitosis	
		Male	Female	Male	Female	Male	Female	Male	Female	Male	Female	Male	Female
5 Min	Control	0, 0, 0	0, 0, 0	0, 0, 0	0, 0, 0	0, 0, 0	0, 0, 0	0, 0, 0	0, 0, 0	0, 0, 0	0, 0, 0	0, 0, 0	0, 0, 0
	PEG-R-Si-Au-NP	**1, 1, 1**	**1, 1, 1**	**0, 0, 0**	**0, 0, 0**	**0, 0, 0**	**0, 0, 0**	**0, 0, 0**	**0, 0, 0**	**0, 0, 0**	**0, 0, 0**	**0, 0, 0**	**0, 0, 0**
2 Hours	Control	0, 0, 0	0, 0, 0	0, 0, 0	0, 0, 0	0, 0, 0	0, 0, 0	0, 0, 0	0, 0, 0	0, 0, 0	0, 0, 0	0, 0, 0	0, 0, 0
	PEG-R-Si-Au-NP	**2, 2, 2**	**2, 2, 2**	**1, 1, 2**	**2, 2, 2**	**0, 0, 0**	**0, 0, 0**	**0, 0, 0**	**0, 0, 0**	**0, 0, 0**	**0, 0, 0**	**0, 0, 0**	**0, 0, 0**
24 Hours	Contrel	0, 0, 0	0, 0, 0	0, 0, 0	0, 0, 0	0, 0, 0	0, 0, 0	0, 0, 0	0, 0, 0	0, 0, 0	0, 0, 0	2, 2, 2	2, 2, 2
	PEG-R-Si-Au-NP	**1, 1, 1**	**1, 1, 1**	**2, 2, 2**	**2, 2, 2**	**0, 0, 0**	**0, 0, 0**	**2, 1, 1**	**2, 2, 2**	**0, 1, 1**	**0, 1, 1**	**1, 0, 0**	**0, 1, 0**
1 Week	Control	0, 0, 0	0, 0, 0	0, 0, 0	0, 0, 0	0, 0, 0	0, 0, 0	0, 0, 0	1, 1, 0	0, 0, 0	1, 1, 0	1, 1, 1	1, 1, 1
	PEG-R-Si-Au-NP	**0, 0, 0**	**0, 0, 0**	**2, 2, 2**	**2, 1, 2**	**0, 0, 0**	**0, 0, 0**	**0, 0, 0**	**0, 0, 0**	**0, 0, 0**	**0, 0, 0**	**2, 2, 2**	**1, 1, 2**
2 Weeks	Control	0, 0, 0	0, 0, 0	0, 0, 0	0, 0, 0	0, 0, 0	0, 0, 0	0, 0, 0	0, 0, 0	0, 0, 0	0, 0, 0	0, 0, 0	0, 0, 0
	PEG-R-Si-Au-NP	**0, 0, 0**	**0, 0, 0**	**2, 2, 2**	**2, 2, 2**	**0, 0, 0**	**0, 0, 0**	**1, 1, 1**	**0, 1, 0**	**0, 0, 1**	**0, 0, 0**	**0, 0, 0**	**0, 0, 0**

IR Group

		Pigment in Sinusoids		Pigment in Macrophages		Pigment in Hepatocytes		Apoptosis		Necrosis		Mitosis	
		Male	Female	Male	Female	Male	Female	Male	Female	Male	Female	Male	Female
5 Min	Control	0, 0, 0	0, 0, 0	0, 0, 0	0, 0, 0	0, 0, 0	0, 0, 0	0, 0, 0	0, 0, 0	0, 0, 0	0, 0, 0	0, 0, 0	0, 0, 0
	PEG-R-Si-Au-NP	**0, 0, 0**	**0, 0, 0**	**0, 0, 0**	**0, 0, 0**	**0, 0, 0**	**0, 0, 0**	**0, 1, 0**	**0, 0, 0**	**0, 0, 0**	**0, 0, 0**	**0, 0, 0**	**0, 0, 0**
2 Hours	Control	0, 0, 0	0, 0, 0	0, 0, 0	0, 0, 0	0, 0, 0	0, 0, 0	0, 0, 0	0, 0, 0	0, 0, 0	0, 0, 0	0, 0, 0	0, 0, 0
	PEG-R-Si-Au-NP	**0, 0, 0**	**0, 0, 0**	**0, 0, 0**	**0, 0, 0**	**0, 0, 0**	**0, 0, 0**	**0, 0, 0**	**0, 0, 0**	**0, 0, 0**	**0, 0, 0**	**0, 0, 0**	**0, 0, 0**
24 Hours	Contrel	0, 0, 0	0, 0, 0	0, 0, 0	0, 0, 0	0, 0, 0	0, 0, 0	0, 0, 0	0, 0, 0	0, 0, 0	0, 0, 0	0, 0, 0	0, 0, 0
	PEG-R-Si-Au-NP	**0, 0, 0**	**0, 0, 0**	**0, 0, 0**	**0, 0, 0**	**0, 0, 0**	**0, 0, 0**	**0, 0, 0**	**0, 0, 0**	**2, 0, 0**	**0, 0, 0**	**0, 0, 0**	**0, 0, 0**
1 Week	Control	0, 0, 0	0, 0, 0	0, 0, 0	0, 0, 0	0, 0, 0	0, 0, 0	0, 0, 0	0, 0, 0	0, 0, 0	0, 0, 0	2, 2, 2	1, 1, 1
	PEG-R-Si-Au-NP	**0, 0, 0**	**0, 0, 0**	**0, 0, 0**	**0, 0, 0**	**0, 0, 0**	**0, 0, 0**	**0, 0, 0**	**0, 0, 0**	**0, 0, 0**	**0, 0, 0**	**0, 0, 1**	**1, 1, 0**

IR Group		Pigment in Sinusoids		Pigment in Macrophages		Pigment in Hepatocytes		Apoptosis		Necrosis		Mitosis	
		Male	Female	Male	Female	Male	Female	Male	Female	Male	Female	Male	Female
2 Weeks	Control	0, 0, 0	0, 0, 0	0, 0, 0	0, 0, 0	0, 0, 0	0, 0, 0	1, 0, 0	0, 0, 0	1, 0, 0	0, 0, 1	0, 0, 0	0, 0, 0
	PEG-R-Si-Au-NP	**0, 0, 0**	**0, 0, 0**	**0, 0, 0**	**0, 0, 0**	**0, 0, 0**	**0, 0, 0**	**0, 0, 0**	**0, 1, 0**	**0, 0, 0**	**0, 0, 0**	**0, 0, 0**	**0, 0, 0**

Sci Transl Med. Author manuscript; available in PMC 2013 December 26.